Energy Conversion and Management 117 (2016) 12–20

Contents lists available at ScienceDirect

Energy Conversion and Management

journal homepage: www.elsevier.com/locate/enconman

Design of a SOFC/GT/SCs hybrid power system to supply a rural isolated microgrid

Haritza Camblong [a,*], Sylvain Baudoin [a,b,c], Ionel Vechiu [b], Aitor Etxeberria [a,b]

[a] Department of Systems Engineering & Control, University of the Basque Country, (UPV/EHU), Europa Plaza 1, E-20018 Donostia, Spain
[b] ESTIA Institute of Technology, Technopole Izarbel, F-64210 Bidart, France
[c] IMS, Bordeaux University, 351 cours de la Libération CS 10004, F-33405 Talence, France

ARTICLE INFO

Article history:
Received 21 December 2015
Accepted 2 March 2016

Keywords:
Hybrid power system
SOFC
Gas microturbine
Supercapacitors module
Multilevel 3LNPC converter
Robust digital controller

ABSTRACT

The aim of this research study has been to design a Hybrid Power System (HPS) which works with biogas and whose main components are a Solid Oxide Fuel Cell (SOFC), a Gas microTurbine (GT), and a module of SuperCapacities (SCs). The HPS is the only power source of a rural isolated microgrid. Its structure, operating strategy, and controller have been designed considering the following criteria: efficiency, power quality, SOFC lifetime and robustness in stability and performance.

The HPS structure includes a unique power converter, a 3-Level Neutral Point Clamped (3LNPC) inverter that connects the HPS to the AC microgrid. Regarding the selected operating strategy, it consists in regulating the SOFC power output to its rated value. Thus, the SCs and the GT must respond to the power demand variations. On the other hand, a study of the HPS shows that its dynamic behavior is not linear. Therefore, a special attention is put on designing a robust HPS controller. The control model is identified and the robust digital controller is designed using the “Tracking and Regulation with Independent Objectives” method. Simulation and experimental results show how the proposed structure, operating strategy, and controller allow ensuring a good behavior of the HPS from the point of view of the above-mentioned four criteria.

1. Introduction

Rural sites are relatively often isolated from an electrical point of view. In developed countries, there are sites where the grid is weaker and where it fails more easily than in urban areas. On the other hand, in developing countries, many rural regions are not connected to the main grid. Thus, rural regions are the type of areas where grids or microgrids are most often islanded or isolated from the main grid.

Many isolated microgrids operate with fossil fuels based power sources, especially with diesel engines. On top of being pollutant, these resources are usually not available locally, and thus, their transport increases the local electricity production cost. Nevertheless, rural regions are richly endowed with renewable resources. Some, as wind or sun resources, are intermittent. In consequence, the microgrid cannot be based only on them. However, in rural and particularly agricultural areas, biomass-based resources are usually abundant. One of them is the biogas produced from the degradation of organic waste. As opposed to other renewables, biogas can be stored in order to produce the demanded power anytime [1]. Moreover, it offers an additional revenue stream to the farmer.

The most used technology to produce electricity from biogas is the classical combustion engine. According to [2], its power range is generally from 10 kW to 5 MW, but power values out of this range also exist [3,4]. The classical combustion engine cost is around 1000 €/kWe [5]. Its electrical efficiency depends on the installed power [6,7] and it is not very good: 20–25% for a rated power of 5 kW and 43% when it is higher than 500 kW.

In fact, in order to obtain a good electrical efficiency, different complementary technologies have to be employed, with the objective of transforming as much as possible the excess heat in electricity. In a hybrid power system formed by a Solid Oxide Fuel Cell (SOFC) and a Gas microTurbine (GT), both power sources use the same gas cycle to generate electricity [8]. Indeed, the SOFC output gases are burned to feed the GT. Reusing the hot gases emitted by the GT, a theoretical electric efficiency of 70% can be reached [9]. In addition, the biogas can directly feed the combustion chamber upstream the GT which allows modifying the overall produced power independently of the SOFC operation. However, feeding biogas directly to the GT decreases the electric efficiency of the hybrid power system.

* Corresponding author. Tel.: +34 943018681.
E-mail address: a.camblong@ehu.eus (H. Camblong).

http://dx.doi.org/10.1016/j.enconman.2016.03.006
0196-8904/

Many studies deals with the thermodynamics of the SOFC/GT hybrid system, for instance [10,11], but very few [12] consider the electric dynamics of the load behavior which can be critical in an isolated context. One objective of this paper is to contribute to the study of the SOFC/GT hybrid system from an electric point of view.

For now, the investment cost of a SOFC is relatively high (around 4500 €/kWe [3,13]), but it could be around 2200 €/kWe [13] when it will be profusely commercialized. Despite a higher investment cost, the overall life cycle cost of such a system is interesting [13] because the maintenance cost of a SOFC (0.5 c€/kWhe [3]) is much lower than that of a combustion engine (1.3 c€/kWhe [3]). Concerning the GT, its investment cost is already competitive (around 1800 €/kWe [3]) comparing with the classical combustion engines. Moreover, a GT requires a lower maintenance (1 c€/kWhe [3]) than a classical combustion engine. For these reasons, and thanks to its higher electric efficiency, a SOFC/GT hybrid system could achieve a very competitive life cycle cost when commercialized.

In addition to the efficiency, the power quality, impact on the equipment aging, and stability and performance robustness are important issues in the operation of a power source, especially in isolated microgrids where operating constraints are more severe.

Regarding the power quality, two characteristics are typically considered to be important: the transient voltage variation and the harmonic distortion of the grid voltage [14–16]. Their importance is even higher in isolated or islanded microgrids. Concerning transients, the abovementioned hybrid power system is not able to ensure quick power changes. Thus, for a standalone operation as in an isolated microgrid, another technology should be considered to meet fast disturbances. Concerning harmonic distortions, they are mostly caused by the inverter used to connect the hybrid power system to the microgrid.

On the other hand, maintenance costs are usually higher in rural areas. It is the reason for which the lifetime and the reliability of a power supply are important parameters to be considered in this context. SOFC power sources lifetime and performance are particularly sensible to the variations of the current they produce [17], especially when these variations are fast [18]. Thus, it is important to avoid the variations.

As most real systems, power sources have usually non-linear and/or non-stationary behaviors. Consequently, power source controllers have to be robust enough to ensure the stability and performance of the power sources in the entire range of operation. Considering that in isolated microgrids the operating point varies faster and more often, and that there are more disturbances than in other grids, robustness is even more important in isolated microgrids.

In this research study, a novel Hybrid Power Source (HPS) and its related operating strategy and controller have been designed in order to address the different issues abovementioned. The proposed solutions allow improving the operating of the HPS in the following areas:

- Efficiency of the HPS.
- Power quality.
- Lifetime of the SOFC.
- Robustness of the HPS stability and performance.

In Section 2 the overall rural microgrid is described after describing and justifying the choice of the HPS structure, including the power electronics topology employed to connect the different components of the HPS to the AC microgrid. In Section 3, the selected operating strategy is discussed. The research study is focused on the operating strategy of the DC side of the inverter connecting the HPS to the microgrid, and it doesn't take into consideration the AC side of the inverter.

In Section 4, the design of the HPS controller is explained. Finally, in Sections 5 and 6, simulation and experimental results are shown, and some conclusions and perspectives about the carried out research study are given.

2. HPS structure and studied rural isolated microgrid

2.1. Design of the HPS structure

Power converters manage the power generated by each component of the HPS and connect the HPS to the microgrids. Fig. 1 shows three possible power electronics topologies to connect a SOFC, GT, and the grid.

In the first topology (a), a DC/DC boost converter allows increasing the SOFC voltage and controlling its power. Then, the two DC buses are connected to the grid through two inverters. As a result switching losses are relatively high.

In the second topology (b) two DC/DC converters allow controlling the power produced by each power source and a shared inverter makes the connection to the grid. This solution is more interesting because it avoids the synchronization of inverters that is necessary in topology (a).

The third topology (c) uses only two converters, instead of three. Thus, switching losses are reduced. Nevertheless, this configuration does not allow controlling independently the power produced by each power source.

A fourth possible topology is based on the use of a multilevel inverter, such as the 3-Level Neutral Point Clamped (3LNPC), as shown in Fig. 2. This type of inverter is able to adjust the current split between the two DC branches through an offset added to the modulation signals, avoiding using more DC/DC and DC/AC converters. Consequently, the power electronics topology proposed in Fig. 2 reduces significantly the power losses due to transistor switching, increasing the overall efficiency of the system compared to the other topologies. Moreover, a multilevel inverter such as the 3LNPC inverter causes less harmonic distortions than a classical inverter [19]. Considering these advantages, the power electronics topology of Fig. 2 is used for the HPS.

Since the 3LNPC causes current fluctuations at three times the grid frequency in its DC side [20], the power produced by the SOFC oscillates at this frequency. This fact has a negative effect on the lifetime and performance of the SOFC [17,18]. Furthermore, the behavior of the current or power split carried out through the offset is not linear [21] and depends, among others parameters, on the microgrid impedance module and phase. This non-linear behavior makes it more difficult to achieve robustness in stability and performance. Consequently, these issues have to be considered in the design of the HPS controller.

On the other hand, as aforementioned, the SOFC/GT hybrid power system is not able to ensure fast power changes. To respond to fast disturbances or load variations a SuperCapacitors module (SCs) can be added to the HPS, as shown in Fig. 2. Installed in parallel with the GT, the SCs can compensate the low dynamics of the GT. As a result, the proposed HPS in this research work is composed by a SOFC, a GT and a module of SCs. The capacitor C_1 and C_2 are used to filter the fluctuations caused by the inverter switches in the DC bus voltage V_{DC}. V_{GT} is the voltage of the upper DC bus and V_{SOFC} is the voltage of the lower one. The names subscripts of the currents flowing in the DC side of the inverter are the name of the component or branch from which they flow.

2.2. Description of the studied rural isolated microgrid

As the authors did in a previous work [22], the analyzed rural isolated microgrid (Fig. 3) has been defined using data from different scientific studies. It contains a unique power source, the HPS,

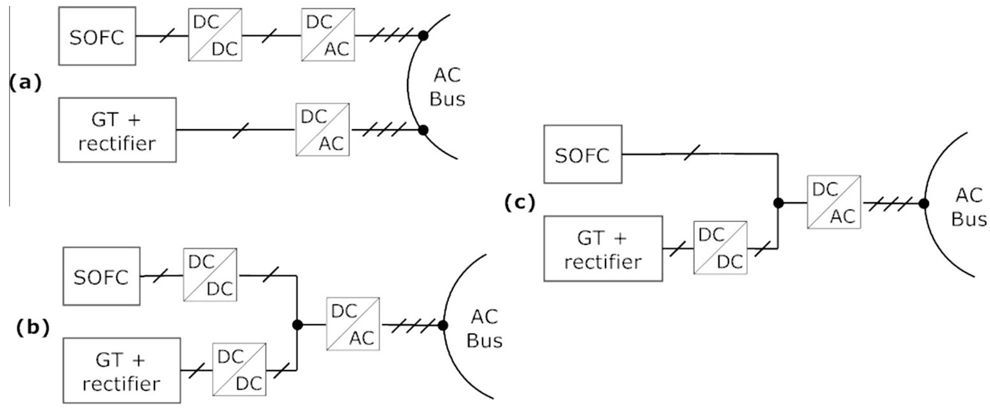

Fig. 1. Different power converters' topologies to connect the HPS components: (a) separated, (b) parallel, (c) floating.

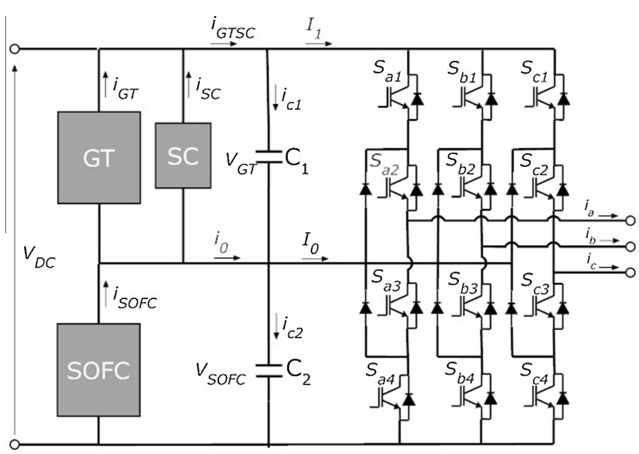

Fig. 2. Schematic representation of the HPS associated to a 3LNPC converter.

Table 1
Definition and values of the components' parameters.

Name	Definition	Value
$P_{SOFC(nom)}$	SOFC nominal power	60 kW
$P_{GT(nom)}$	GT nominal power	30 kW
$P_{GT(min)}$	GT minimal power	15 kW
$P_{ld(min)}$	Minimum load power the HPS can supply	75 kW
$P_{ld(max)}$	Maximum load power the HPS can supply	90 kW
C_{SC}	SCs module capacitance	5.74 F
$V_{SC(max)}$	SCs module maximum voltage	534.6 V
R_{SC}	SCs module resistor	81.4 mΩ
V_{DC}	DC nominal voltage	1000 V
C_1, C_2	DC bus filter capacitors	91 mF
L_f	Inverter-side inductance of the AC side filter	270 μH
C_f	Capacitor of the AC side filter	82 μF
f_g	3-phase AC microgrid nominal frequency	50 Hz
V_g	3-phase AC microgrid nominal voltage	400 V
Z_1	Impedance of the line between the 3-LNPC and the first load	(0.11 + 0.018i) Ω
Z_2	Impedance of the line between the first and the second load	(0.055 + 0.0088i) Ω
L_{d1}	First load impedance	2.12 Ω
L_{d2}	Second load impedance	(10.6 + 14.1i) Ω

and two loads. An AC inductance-capacitor-inductance (LCL) filter is placed at the output of the inverter. Regarding the length of the electric lines, the distance between the HPS and the first load is 200 m, and there are 100 m more to the second load. These are typical values in rural areas. Also, being a low voltage weak grid, the distribution lines are very resistive [23].

While the components of the HPS have been sized to maximize the overall efficiency of the system, as explained in [22], the SCs capacity has been sized to compensate the relatively low dynamics of the GT. Table 1 shows the definition and the values of the components' parameters.

The HPS and the rural isolated microgrid have been modeled in Matlab/Simulink using different data from the scientific literature [22].

3. Operating strategy

The operating strategy of the HPS is based on regulating the SOFC power to its rated value ($P_{SOFC}^{ref} = 60$ kW) and responding to load variations with the GT and SCs. There are four reasons which justify regulating the SOFC to its rated value:

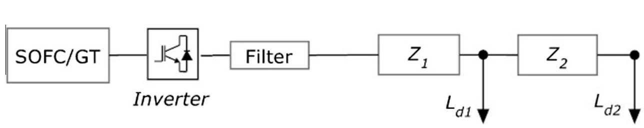

Fig. 3. Rural isolated microgrid schema.

- Changes in the temperature of the SOFC are directly linked to load variations and they negatively affect the SOFC lifetime and performance [17].
- SOFC power varies slowly because the power produced depends on the temperature of the cell [24]. Thus, the settling time of the SOFC is not sufficient to feed isolated loads.
- Sudden power variations of the SOFC could deteriorate its performance [18].
- The efficiency of the SOFC in partial load is relatively low [25] compared with that of the GT [26].

As aforementioned, the offset added to the 3LNPC inverter modulation index allows controlling the current split between the two DC buses. When the offset is positive, the 3LNPC inverter lets flow more I_1 current through the upper DC bus, thus increasing i_{GTSC}, at the expense of reducing the current of the lower DC bus, I_0, thus decreasing i_{SOFC} (Fig. 2) [19]. This offset can be used to regulate the SOFC power. For instance, when the load power increases, the offset should also increase making the GT and the SCs supply more power.

The overall HPS operating and control strategy is shown in Fig. 4. The GT power output is controlled by the controller included in the commercial *Capstone C30* GT, through solenoid valves that regulate the gas flow entering the combustion chamber (CC in

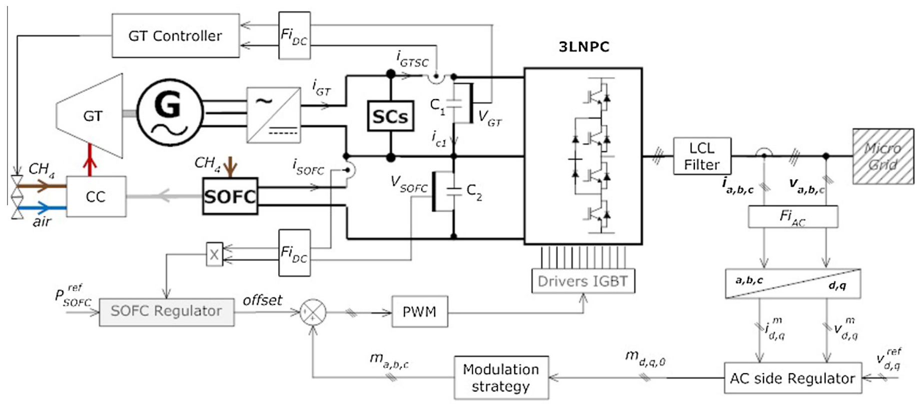

Fig. 4. Global control schema of the HPS.

Fig. 4) [27,28]. The GT power reference is calculated multiplying the upper DC bus voltage V_{GT} and the current I_{GTSC}, which comes from the GT and the SCs. V_{SOFC} is the lower DC bus voltage, of the SOFC. $i_{a,b,c}$ and $v_{a,b,c}$ are respectively the 3-phase current and voltage measured at the output of the LCL filter. $i^m_{d,q}$ and $v^m_{d,q}$ are the projection of $i_{a,b,c}$ and $v_{a,b,c}$ in the (d,q) reference frame. $v^{ref}_{d,q}$ and $m_{d,q,0}$ are the voltage references and the inverter modulation signals respectively in the (d,q) reference frame and $m_{a,b,c}$ are the modulation signals in the (a,b,c) reference frame.

As shown in Fig. 4, voltage and current measures are processed by low-pass filters (F_{iDC} and F_{iAC}), before being used by the controller.

4. Controller design

In order to design a good controller, three fundamental elements are needed [29]:

- A specification of the closed-loop (CL) desired performance.
- A control model, i.e. a model used to design the controller.
- A designing method consistent with the control model and the desired performance.

In order to define the controller specifications, the next section analyses the system that is controlled.

4.1. Analysis of the system

As aforementioned, the operating strategy of the HPS is to regulate the SOFC power to its nominal value through the offset added to the modulation index of the 3LNPC inverter. Before designing the controller, the system under control is analyzed in this section, in order to specify the desired controller performance. The system input is the offset and the output is the SOFC power.

The behavior of the current split created by the offset is not linear [21]. This current split behavior depends on the grid impedance module and phase, among others parameters. Since the SOFC power is related to the current split, the system is also non-linear.

The dynamic behavior between the offset and the SOFC power is analyzed in a simulation, by applying an offset step with an amplitude of 0.1 in $t = 0.3$ s. This test is performed at two different operating points, when the load level P_{Ld} 75 kW and 90 kW. The results are shown in Fig. 5, where a non-linear behavior is clearly observed. The gain of the system is bigger when the load is bigger. The 5% settling time also varies depending on the operating point. For $P_{Ld} = 75$ kW it is approximately 24 ms, and for $P_{Ld} = 90$ kW it is approximately 26 ms. Furthermore, oscillations at 150 Hz (3 times f_g) with a big amplitude of 1.5 kW are visible at both operating points. These oscillations are due to the 3LNPC inverter structure [20], and they can adversely affect the performance and lifetime of the SOFC [17,18].

4.2. Definition of the controller specifications

Since the operating strategy's goal is to regulate the SOFC power to its rated value, the controller first objective is a zero static error.

For the CL dynamic behavior the following specifications are defined:

- Oscillations at 150 Hz have to be damped as much as possible.
- The transient response has to be not too fast. First, because the offset is added to the 3LNPC modulation index. This index is used to regulate the AC frequency and voltage with a settling time of 1–2 ms. In order to uncouple the control of the DC and AC sides, the settling time of the two related CL systems has to be different. Secondly, it is recommended that the SOFC power variations should not be too fast, in order to prevent damaging the SOFC. Thus, the desired tracking and regulation dynamic behavior is of second order, with a damping factor of 0.7 and a 5% settling time of 10 ms.

Finally, taking into account the non-linearity of the system and the high number of parameters affecting this non-linearity, the controller has to be robust to ensure that within the entire operating range there is:

- Stability.
- Robustness in stability.
- Wherever possible, constant dynamic performance.

This way, the controller has to meet the standard robustness margins in the entire operating range.

4.3. Sampling time and anti-aliasing filters

Since the controller has to be implemented in a digital processor, its sampling time must be defined. On the other hand, in this research study, the controller is directly designed as digital, thanks to a digital control model, without the design of a previous continuous controller. The direct digital design has some advantages [29]:

- The selected sampling time is lower, thus requiring a lower processing power.
- The real robustness of the controller can be considered in the design of the controller.
- Once designed, the controller can be directly implemented.

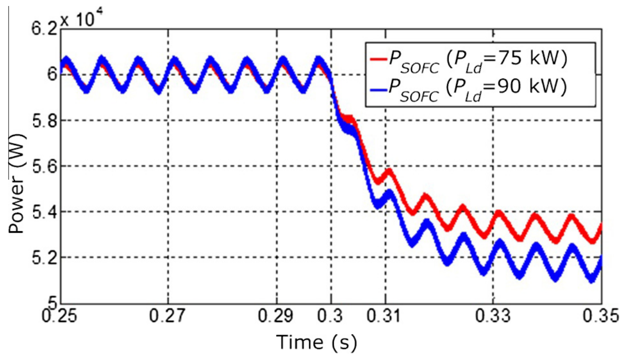

Fig. 5. Response of the SOFC power output to an offset step of amplitude +0.1 at $t = 0.3$ s, for two load levels: 75 kW and 90 kW.

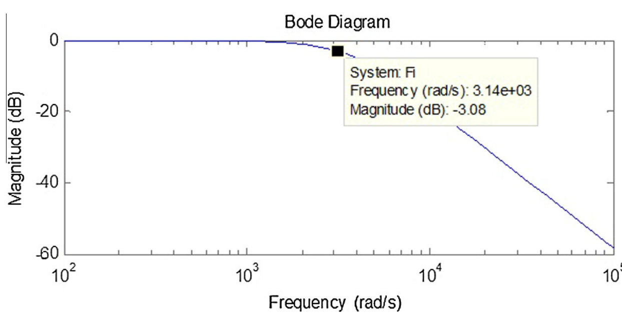

Fig. 6. Bode diagram of the F_{iDC} filter.

When using this design process, the sampling frequency f_s must comply with the following condition [29]:

$$6 \cdot f_{CLBW} \leqslant f_s \leqslant 25 \cdot f_{CLBW} \tag{1}$$

where f_{CLBW} is the CL bandwidth. Considering the specified dynamic behavior, this bandwidth is more or less of 50 Hz. Thus, a sampling frequency of 1 kHz is chosen, 20 times f_{CLBW}, allowing reducing a bit the desired settling time if necessary in the controller adjustment process. On the other hand, f_s being largely greater than twice the oscillations frequency of 150 Hz, the digital controller is able to damp these oscillations.

The anti-aliasing filter F_{iDC} is of second order with a bandwidth of 495 Hz. Its Bode diagram is shown in Fig. 6. At 150 Hz, the attenuation is only -0.17 dB.

4.4. Identification of the control model

The relation between the offset applied to the 3LNPC inverter and the SOFC power is very complex and cannot be expressed analytically. In order to obtain the control model, an identification process is carried out. The identification is made meeting the following conditions:

- The AC side controller is operating at a constant power and with a settling time allowing decoupling the behaviors of the AC and DC side.
- The operating point corresponds to:
  - A balanced and constant DC voltage at 1000 V.
  - A resistive AC load of 90 kW. This power level corresponds to the highest gain of the system to be controlled. Thus, securing standard robustness margins in this operating point ensures meeting them in the entire operating range.
- The offset signal is a pseudo random binary signal (PRBS) [29] of $N = 10$ bits, with a mean value of 0.18 which corresponds to the nominal power split 30/60 kW, and amplitude of 0.15.

Once the experimental identification process completed, the control model between the offset and the SOFC power P^m_{SOFC} is obtained thanks to the System Identification Toolbox of Matlab. The control model is of third order:

$$\frac{P^m_{SOFC}}{offset} = \frac{-7521z^{-1} + 8616z^{-2} - 7461z^{-3}}{1 - 2.077z^{-1} + 2.059z^{-2} - 0.9016z^{-3}} \tag{2}$$

The control model Bode diagram is shown in Fig. 7. It can be seen that the resonance at 150 Hz has been correctly identified.

4.5. Design of the controller

Since the controller is digital, single-input–single-output type and linear, it is represented in the RST canonic form (see Fig. 8), where R, S, T, B_m and A_m are polynomials in the digital delay operator q^{-1} [29]. In Fig. 8, B and A are the numerator and denominator of the control model, P^m_{SOFC} is the SOFC power reference (ie 60 kW) and P_y represents the disturbances in the output of the system.

Fig. 9 shows the control model roots and zeros position on the Z digital plan. It can be observed that they are inside the unity circle, i.e. stable. Thus, they can be cancelled out thanks to the RST controller. This is the reason the "Tracking and regulation with independent objectives" method is used to adjust the controller [29].

For the design of the controller, dominant poles included in P_D polynomial are chosen to meet the dynamic specifications. Furthermore, two damped (damping factor of 0.1) auxiliary poles (P_F polynomial) are added in the desired CL characteristic polynomial in order to limit the attenuation of the transfer function, also named sensitivity function, S_{yp}, between the disturbances P_y and the measured SOFC power signal P^m_{SOFC} at 150 Hz. Thus, the desired CL characteristic polynomial is:

$$P(q^{-1}) = P_D(q^{-1})P_F(q^{-1}) \tag{3}$$

A property related to S_{yp} states that the integral in frequency of its gain is constant. Moreover, it can be demonstrated that the modulus margin, the most global robustness margin, is equal to the inverse of the maximum gain of S_{yp} [29]. Thus, a limitation of the attenuation of S_{yp} at 150 Hz is implemented to increase slightly the gain of S_{yp} at 150 Hz and so to decrease the S_{yp} maximum gain. This way, the modulus margin is increased. The Bode diagram of S_{yp} is depicted in Fig. 10 where the disturbances at 150 Hz are significantly attenuated even with the auxiliary poles.

The polynomials R, S, T, B_m and A_m obtained with this adjustment are:

$$R(q^{-1}) = 0.4231 - 0.9573q^{-1} + 0.9474q^{-2} - 0.3579q^{-3} \tag{4}$$

$$S(q^{-1}) = -7521 + 16138q^{-1} - 16078q^{-2} + 7461q^{-3} \tag{5}$$

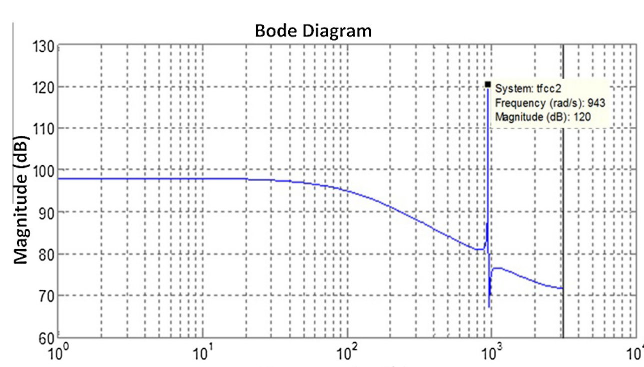

Fig. 7. Bode diagram of the identified control model.

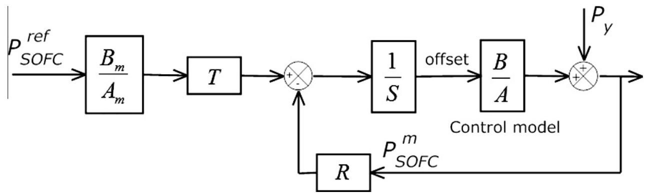

Fig. 8. Blocs diagram of the RST controller.

$$T(q^{-1}) = 1 - 2.6534q^{-1} + 3.1784q^{-2} - 2.0133q^{-3} + 0.5437q^{-4} \tag{6}$$

$$B_m(q^{-1}) = 0.2592 \tag{7}$$

$$A_m(q^{-1}) = 1 - 0.7408q^{-1} \tag{8}$$

The modulus margin is −2.19 dB (according to standards it has to be greater than −6 dB) and the delay margin is 1.03 T_s (according to standards it has to be greater than T_s), where T_s is the sampling time.

5. Simulation results

Simulations have been carried out on a validated model of the HPS. This model has been implemented in a real time OPAL RT simulator [22]. The model and control laws have been executed in three different cores with distinct processing time (Fig. 15): the parts of the model with low dynamics (thermal and chemical ones) at 200 µs, the electrical dynamics at 1 µs, and the control laws at T_s (200 µs for the AC side controller).

The HPS has been tested in the most constraining case in order to test its robustness. Two load steps are applied at t = 150 s and t = 200 s. In the first event, the demanded power varies from 90 kW to 75 kW, and in the second from 75 kW to 90 kW, covering the entire defined operating range. Fig. 11 shows that the SOFC power is maintained at its rated value as expected, with a zero static error. Thanks to its fast dynamics, the SCs module allows responding to the fast variation of the demand while the GT power reaches its power reference with slower dynamics.

Fig. 12 shows the voltage variations of two DC buses. When the SCs module is charged in t = 150 s, the upper DC bus voltage V_{GT}, which is also the SCs voltage, increases. Conversely, when the SCs module is discharged in t = 200 s, the voltage decreases.

Fig. 13 shows the two transient responses of the SOFC power. The maximum peak is 4.5% of the SOFC rated power. In both cases, the 5% settling time obtained is approximately 10 ms, as desired. Regarding the steady state behavior, oscillations at 150 Hz still exist, but they are significantly smaller (0.4 kW versus 1.5 kW in open loop). Other tests have proven that these oscillations could be damped even more by adjusting the controller, but this saturates the offset at certain point.

6. Experimental results

6.1. Configuration of the experimental system

The HPS model used for simulations has been implemented in the real-time simulator Hardware-In-the-Loop (HIL) OP 5600 HILbox OPAL RT, in order to emulate the behavior of the HPS in the EneR-GEA experimental platform [30]. The HIL simulator has a large computing capacity spread over four 2.4 GHz processors, which allow running real-time simulations with calculation steps up to 10 µs. The HIL interface runs under Matlab/Simulink and includes among others the field-programmable gate array type programmable integrated circuit to generate high frequency pulse width modulation signals (several decades kHz).

As shown in Fig. 14, the HPS model simulated in real time with the HIL system generates the voltage signals $V_{GT(c)}$ and $V_{SOFC(c)}$, which are the 2 voltage references of the power amplifiers. Thus, the amplifiers generate the voltage of the two DC buses. The bus of the SCs and GT is above, and the bus of the SOFC is below. The HIL system is also used to control the switches of the 3LNPC converter. In addition, the anti-aliasing filters F_{iDC} and F_{iAC} filter the measured analog signals before they are sampled. The inputs and outputs of the HIL system are:

- 2 analog voltage outputs representing the two power sources of the hybrid system model: the SOFC and the GT associated with the SCs module.
- 12 digital outputs to control the switches of the 3LNPC.
- One digital output signal to control a switch that can add a second load to the microgrid.
- 10 analog inputs: the phase-neutral voltages $V_{a,b,c}$ and the currents $i_{a,b,c}$ of the three phases, and the current and voltage (V_{GT} and V_{SOFC}) of the two DC buses.

The real components of the experimental platform include the DC side filter, with its capacitors C_1 and C_2, the 3LNPC converter, the LCL filter at the AC side, the power lines (represented by the impedances Z_1 and Z_2) and the loads L_{d1} and L_{d2}.

The HPS model runs on 4 processors of the HIL simulator. As illustrated in Fig. 15, each processor uses a different calculation time step.

The experimental platform cannot operate with the power of the rural microgrid of 100 kW considered in this research study.

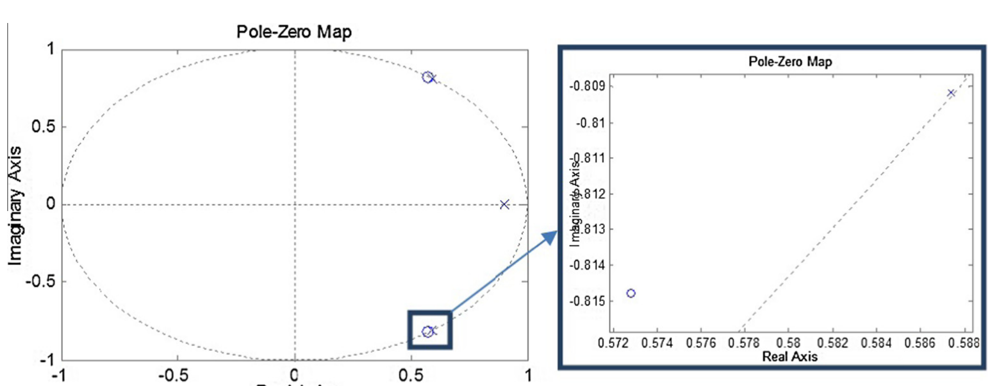

Fig. 9. Control model roots and zeros position on the Z digital plan.

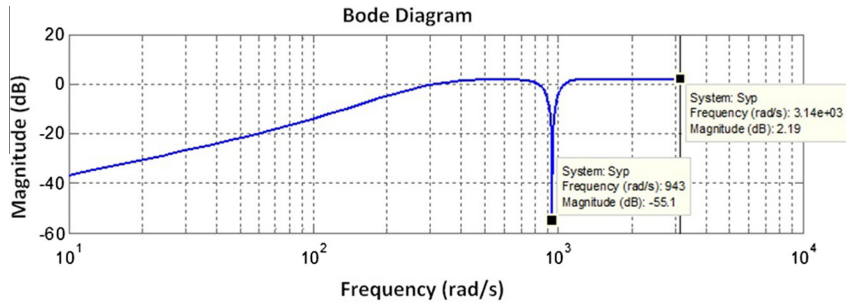

Fig. 10. S_{yp} Bode diagram.

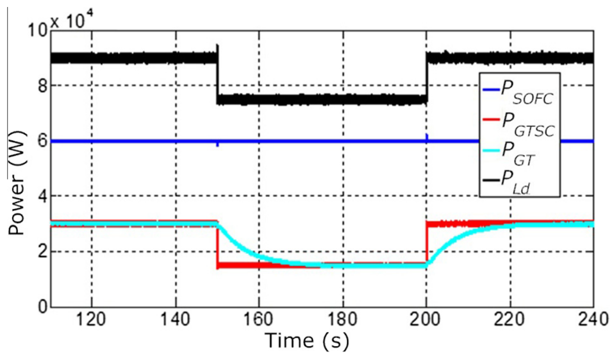

Fig. 11. Evolution of the power of the SOFC, the GT and SCs combined, the GT, and the load in the simulation test.

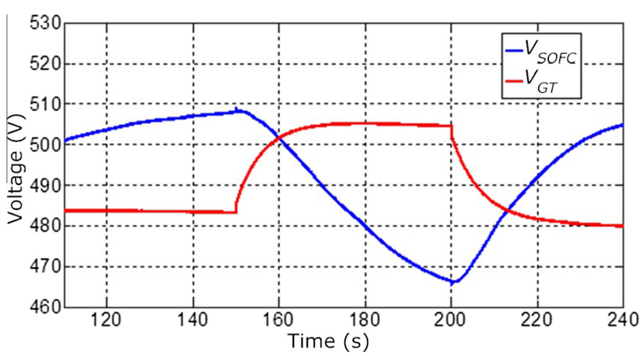

Fig. 12. Evolution of the upper and lower DC buses voltage in the simulation test.

Thus, the experimental tests in this platform are made at reduced power.

The most limiting factor of the experimental setup is the maximum power that the amplifiers can generate. This is 1.5 kW while the maximum power of one of the power sources of the system is 60 kW (SOFC). Using a scaling factor of $K_{ech} = 43$, the power amplifier that represents the SOFC generates a maximum of 1.4 kW. The HPS parameters do not change; they are simulated at real power levels.

The DC and AC side filters' size is changed. The values of the corresponding parameters are given in Table 2. This table gives also the new impedance value of the experimental loads. The lines' impedance has not been measured. The length of these lines is approximately 10 m.

6.2. Experimental tests

The scenario of the experimental test is very similar to that of the simulation. As explained above, the main difference is the power level which is much lower in the experimental platform, with a scale factor of 43 in the current. Another difference is that in the experimental platform, the second load (Fig. 14) is purely resistive. The voltage levels are the same in the experimental platform and the simulation model.

The second load is disconnected from the microgrid at $t = 150$ s, through the contactor of the experimental platform (Fig. 14), and it is connected again at $t = 200$ s.

Fig. 16 shows the evolution of the power of the different components of the HPS during the experimental test. As in the simulation, the SOFC power is regulated to its rated value with zero static error. The power demand variation is ensured first by the SCs module for its fast dynamics, and then by the GT. It has to be noted that the noise level of the measured variables is high. This issue is addressed at the end of the section.

The DC buses voltage evolution presented in Fig. 17 is also similar to that obtained in the simulation. Again, some noise is observable, but it is lower than in the measured power.

The DC voltage levels in the experimental test are slightly different compared to the voltage levels obtained in the simulation: the SOFC voltage is slightly lower in the experimental test while

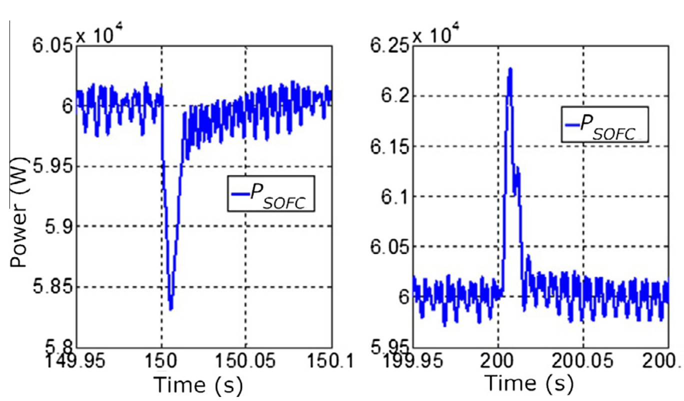

Fig. 13. SOFC power transient response in the simulation test.

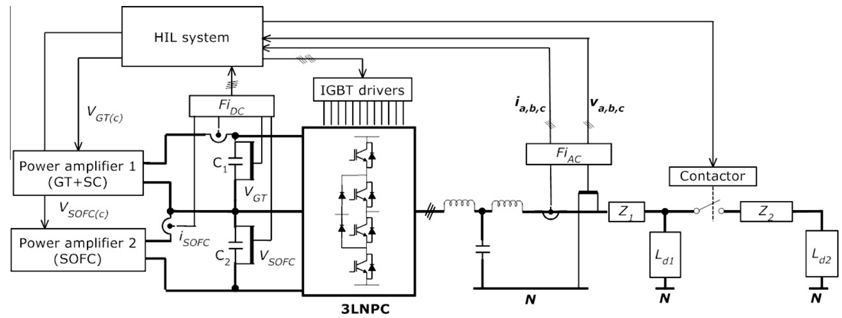

Fig. 14. Schema of the experimental configuration.

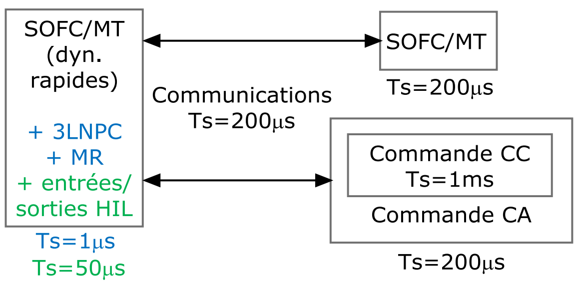

Fig. 15. Separation of the model and the control laws in different cores with distinct processing times in simulation (difference in blue) and experimental (difference in green) tests. (For interpretation of the references to color in this figure legend, the reader is referred to the web version of this article.)

Table 2
Values of the experimental microgrid parameters.

Name	Definition	Value
C_1, C_2	DC bus filter capacitors	3.3 mF
L_f	Inverter-side inductance of the AC side filter	3 mH
C_f	Capacitor of the AC side filter	2 μF
L_{d1}	First load impedance	91.2 Ω
L_{d2}	Second load impedance	433.1 Ω

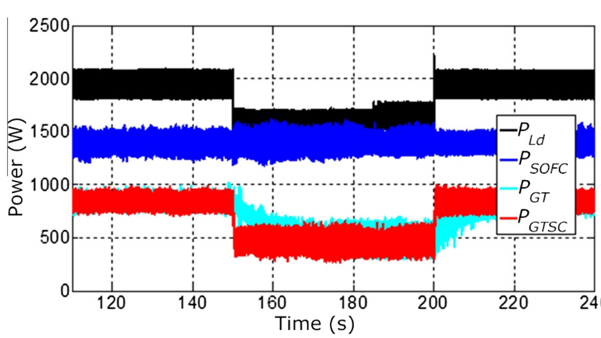

Fig. 16. Evolution of the power of the SOFC, the GT and SCs combined, the GT, and the load in the experimental test.

the GT and SCs voltage is slightly higher. This is because the startup phase in the experimental test is different in the simulation. In particular, as a precaution, the variations of the voltages generated by the power amplifiers have been limited. On the other hand, the SOFC voltage peaks are higher and last more than in the simulation. This can be explained by the abovementioned limitation of the power amplifiers voltage variation.

Regarding the high level noise observed in the experiment, it comes mostly from the measured current. Fig. 18 shows the spectral response of the measured SOFC current at the output of the

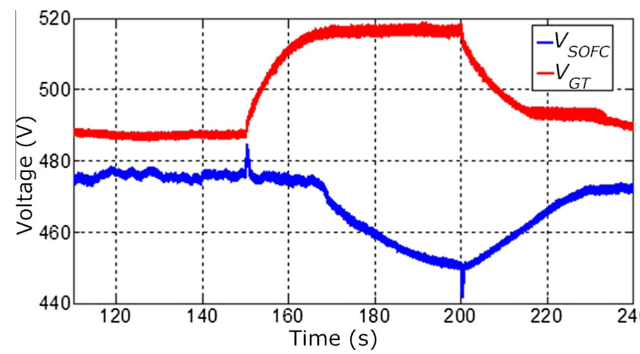

Fig. 17. Evolution of the upper and lower DC buses voltage in the experimental test.

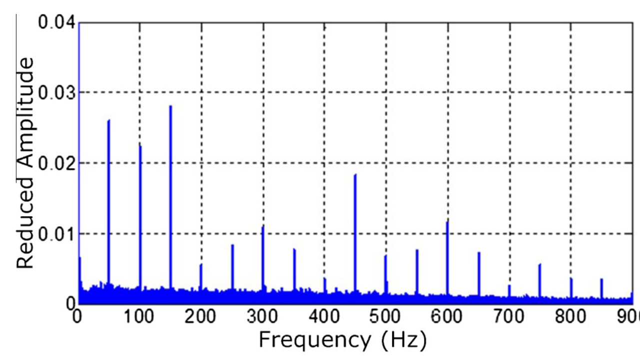

Fig. 18. Spectral analysis of the SOFC current measured in the experimental test.

power amplifier. The noise is concentrated in the microgrid frequency harmonics. Thus, it seems that the origin of this noise is the AC side signals, or a coupling between the power amplifiers and AC side signals. Anyway, it can be observed that the spectral peak at 150 Hz is not significantly higher than at 50 Hz and 100 Hz. Thus, it seems that the oscillations at 150 Hz linked to the structure of the 3LPNPC inverter are damped at a certain level.

7. Conclusions

The research study presented in this paper demonstrates that a well structured, operated and controlled HPS composed by a SOFC, a GT and a SCs module, and connected to the microgrid through a 3LNPC inverter can be a very interesting solution to supply power to rural isolated microgrids where biogas is available.

The designed solution is especially interesting from the point of view of the following criteria:

- Efficiency:
  - The proposed SOFC/GT association and size ensures the maximum conversion of heat into electricity.

  - The chosen power converter topology allows reducing the switching losses and thus increasing the overall efficiency, compared to more classical topologies.
  - Regulating the SOFC to its rated value ensures its maximum efficiency.
- Power quality:
  - The appropriate association of the module of SCs to the hybrid source provides a fast power response capacity to the HPS, allowing managing transients and facing disturbances in an adequate manner.
  - The 3LNPC inverter produces lower harmonic distortions than a classical inverter.
- SOFC lifetime:
  - The strategy of maintaining the SOFC at a constant value improves its lifetime.
  - Thanks to the designed controller, the current oscillations caused by the 3LNPC inverter at three times the microgrid frequency are damped, thus reducing the fatigue of the SOFC.
  - The association of the module of SCs to the hybrid source ensures fast response to power demand variations, avoiding SOFC power fast variations and thus increasing its lifetime.
- Robustness:
  - The design of the robust controller carried out thanks to the identified control model ensures the stability and the performance of the system in all the operating range of the HPS.

The designed HPS has shown its qualities in the scenario considered in this work. However, the behavior of this HPS should be assessed in a more complex microgrid, with other renewable sources and when different events occur. Moreover, an important noise level has been observed in the measures carried out in the experimental test. The origin of this noise has yet not been identified. After identifying it, a solution to decrease this noise should be defined and applied to the experimental platform.

The research group associated to this paper plans to address these two abovementioned issues in future works.

Acknowledgements

The research study described in this paper has been supported by the Basque Coast Adour Agglomeration and ERDF funds.

References

[1] Hahn H, Krautkremer B, Hartmann K, Wachendorf M. Review of concepts for a demand-driven biogas supply for flexible power generation. Renew Sustain Energy Rev 2014;29:383–93. http://dx.doi.org/10.1016/j.rser.2013.08.085.

[2] Lindgren G. Assessment of biogas-fueled electric power systems. Palo Alto, California, USA: EPRI; 2004.

[3] Jatana GS, Himabindu M, Thakur HS, Ravikrishna RV. Strategies for high efficiency and stability in biogas-fuelled small engines. Exp Thermal Fluid Sci 2014;54:189–95. http://dx.doi.org/10.1016/j.expthermflusci.2013.12.008.

[4] Wang Wei, Zuo Zhengxing, Liu Jinxiang. Miniaturization limitations of rotary internal combustion engines. Energy Convers Manage 2016;112:101–14. http://dx.doi.org/10.1016/j.enconman.2016.01.002.

[5] Arespacochaga N, Valderrama C, Peregrina C, Hornero A, Bouchy L, Cortina JL. On-site cogeneration with sewage biogas via high-temperature fuel cells: Benchmarking against other options based on industrial-scale data. Fuel Process Technol 2015;138:654–62. http://dx.doi.org/10.1016/j.fuproc.2015.07.006.

[6] Li D, Sun Y, Kong X, Li L, Yuan Z. The future Of biogas utilizations in China. Int Conf Remote Sens Environ Transp Eng; 2011. p. 7967–70. http://dx.doi.org/10.1109/RSETE.2011.5966298.

[7] Milan C, Stadler M, Cardoso G, Mashayekh S. Modeling of non-linear CHP efficiency curves in distributed energy systems. Appl Energy 2015;148:334–47. http://dx.doi.org/10.1016/j.apenergy.2015.03.053.

[8] Speidel M, Kraaij G, Wörner A. A new process concept for highly efficient conversion of sewage sludge by combined fermentation and gasification and power generation in a hybrid system consisting of a SOFC and a gas turbine. Energy Convers Manage 2015;98:259–67. http://dx.doi.org/10.1016/j.enconman.2015.03.101.

[9] Larminie J, Dicks A. Fuel cell systems explained. John Wiley & Sons; 2003.

[10] Barelli L, Bidini G, Ottaviano A. Part load operation of SOFC/GT hybrid systems: stationary analysis. Int J Hydrogen Energy 2012;37(21):16140–50. http://dx.doi.org/10.1016/j.ijhydene.2012.08.015.

[11] Barelli L, Bidini G, Ottaviano A. Part load operation of a SOFC/GT hybrid system: dynamic analysis. Appl Energy 2013;110:173–89. http://dx.doi.org/10.1016/j.apenergy.2013.04.011.

[12] Wu XJ, Huang Q, Zhu XJ. Power decoupling control of a solid oxide fuel cell and micro gas turbine hybrid power system. J Power Sources 2011;196(3):1295–302. http://dx.doi.org/10.1016/j.jpowsour.2010.07.095.

[13] Strazza C, Del Borghi A, Costamagna P, Gallo M, Brignole E, Girdiniob P. Life cycle assessment and life cycle costing of a SOFC system for distributed power generation. Energy Convers Manage 2015;100:64–77. http://dx.doi.org/10.1016/j.enconman.2015.04.068.

[14] Jenkins N. Embedded generation. IET; 2000.

[15] Peças Lopes JA, Hatziargyriou N, Mutale J, Djapic P, Jenkins N. Integrating distributed generation into electric power systems: a review of drivers, challenges and opportunities. Electr Power Syst Res 2007;77:1189–203. http://dx.doi.org/10.1016/j.epsr.2006.08.016.

[16] Bollen MHJ. What is power quality? Electr Power Syst Res 2003;66:5–14. http://dx.doi.org/10.1016/S0378-7796(03)00067-1.

[17] Angrisani G, Roselli C, Sasso M. Distributed microtrigeneration systems. Prog Energy Combust Sci 2012;38:502–21. http://dx.doi.org/10.1016/j.pecs.2012.02.001.

[18] Stiller C, Thorud B, Bolland O, Kandepu R, Imsland L. Control strategy for a solid oxide fuel cell and gas turbine hybrid system. J Power Sources 2006;158:303–15. http://dx.doi.org/10.1016/j.jpowsour.2005.09.010.

[19] Etxeberria A, Vechiu I, Camblong H, Vinassa J-M. Comparison of three topologies and controls of a hybrid energy storage system for microgrids. Energy Convers Manage 2012;54:113–21. http://dx.doi.org/10.1016/j.enconman.2011.10.012.

[20] Yazdani A, Iravani R. Voltage-sourced converters in power systems: modeling, control, and applications. John Wiley & Sons; 2010.

[21] Etxeberria A, Vechiu I, Camblong H, Kreckelbergh S, Bacha S. Operational limits of a three level neutral point clamped converter used for controlling a hybrid energy storage system. Energy Convers Manage 2014;79:97–103. http://dx.doi.org/10.1016/j.enconman.2013.12.008.

[22] Baudoin S. Étude d'un système hybride pile à combustible/microturbine dans un contexte microréseau rural isolé Ph.D. dissertation. University of Basque Country and University of Bordeaux; 2015.

[23] Majumder R. Modeling, stability analysis and control of microgrid Ph.D. dissertation. Queensland University of Technology; 2010.

[24] Obara S. Dynamic-characteristics analysis of an independent microgrid consisting of a SOFC triple combined cycle power generation system and large-scale photovoltaics. Appl Energy 2015;141:19–31. http://dx.doi.org/10.1016/j.apenergy.2014.12.013.

[25] Nanaeda K, Mueller F, Brouwer J, Samuelsen S. Dynamic modeling and evaluation of solid oxide fuel cell – combined heat and power system operating strategies. J Power Sources 2010;195:3176–85. http://dx.doi.org/10.1016/j.jpowsour.2009.11.137.

[26] Rosa do Nascimento MA, de Oliveira Rodrigues L, dos Santos EC, Batista Gomes EE, Goulart Dias FL, Gutiérrez Velásques EI, et al. Micro gas turbine engine: a review. In: Prog gas turbine perform. InTech; 2013.

[27] Hamilton S. Micro turbine (distributed generation) project. Edison Technology Solutions; 1999.

[28] Yinger RJ. Behavior of capstone and honeywell microturbine generators during load changes. Southern California Edison; 2001.

[29] Landau ID, Zito G. Digital control systems: design, identification and implementation. Springer Science & Business Media; 2007.

[30] Camblong H, Curea O, Llaria A, Hacala A. Research experimental platforms to study microgrids issues. Int J Interact Des Manuf 2015;2015:1–5. http://dx.doi.org/10.1007/s12008-015-0288-x. http://link.springer.com/article/10.1007%2Fs12008-015-0288-x [accessed on 14 12 2015].